1-1-2020

The Large Millimeter Telescope (LMT) Alfonso Serrano: Current Status and Telescope Performance

David H. Hughes
Instituto Nacional de Astrofisica Optica y Electronica

F. Peter Schloerb
University of Massachusetts Amherst

Itziar Aretxaga
Instituto Nacional de Astrofisica Optica y Electronica

Edgar Castillo-Domínguez
SRON Netherlands Institute for Space Research

Miguel Chávez Dagostino
Instituto Nacional de Astrofisica Optica y Electronica

See next page for additional authors

PROCEEDINGS OF SPIE

SPIEDigitalLibrary.org/conference-proceedings-of-spie

The Large Millimeter Telescope (LMT) Alfonso Serrano: current status and telescope performance

Hughes, David, Schloerb, F. Peter, Aretxaga, Itziar, Castillo-Domínguez, Edgar, Chávez Dagostino, Miguel, et al.

David H. Hughes, F. Peter Schloerb, Itziar Aretxaga, Edgar Castillo-Domínguez, Miguel Chávez Dagostino, Edgar Colín, Neal Erickson, Daniel Ferrusca Rodriguez, David M. Gale, Arturo Gómez-Ruiz, José Luis Hernández Rebollar, Mark Heyer, James Lowenthal, Alfredo Montaña, Marcos Emir Moreno Nolasco, Gopal Narayanan, Alexandra Pope, Iván Rodríguez-Montoya, David Sánchez-Argüelles, David Smith, Kamal Souccar, Miguel Velázquez de la Rosa Becerra, Grant W. Wilson, Min S. Yun, "The Large Millimeter Telescope (LMT) Alfonso Serrano: current status and telescope performance," Proc. SPIE 11445, Ground-based and Airborne Telescopes VIII, 1144522 (13 December 2020); doi: 10.1117/12.2561893

SPIE.

Event: SPIE Astronomical Telescopes + Instrumentation, 2020, Online Only

The Large Millimeter Telescope (LMT) Alfonso Serrano: Current Status and Telescope Performance

David H. Hughes[a], F. Peter Schloerb[b], Itziar Aretxaga[a], Edgar Castillo-Domínguez[c], Miguel Chávez Dagostino[a], Edgar Colín[a,d], Neal Erickson[b], Daniel Ferrusca Rodriguez[a], David M. Gale[a], Arturo Gómez-Ruiz[a,d], José Luis Hernández Rebollar [a], Mark Heyer[b], James Lowenthal[e], Alfredo Montaña[a,d], Marcos Emir Moreno Nolasco[a], Gopal Narayanan[b], Alexandra Pope[b], Iván Rodríguez-Montoya[a,d], David Sánchez-Argüelles[a,d], David Smith[f], Kamal Souccar[b], Miguel Velázquez de la Rosa Becerra[a], Grant W. Wilson[b], Min S. Yun[b]

[a]Instituto Nacional de Astrofísica, Óptica y Electrónica (INAOE),Luis Enrique Erro 1, Santa María Tonantzintla 72840, Puebla, Mexico;
[b]Dept. of Astronomy, University of Massachusetts, Amherst, MA, USA;
[c]SRON-Netherlands Institute for Space Research, Landleven 12, 9747 AD Groningen, Netherlands
[d] Consejo Nacional de Ciencia y Tecnología, Av. Insurgentes Sur 1582, Col. Crédito Constructor, Alcaldía Benito Juárez, C.P. 03940, Ciudad de México, México
[e]Smith College, Northampton, MA 01063, USA
[f]MERLAB P.C. & Georgia Institute of Technology, Georgia, USA

ABSTRACT

The Large Millimeter Telescope (LMT) Alfonso Serrano is a 50m-diameter single-dish radio telescope constructed at an altitude of 4600 meters on the summit of Volcán Sierra Negra, an extinct volcano in the Mexican state of Puebla. The LMT is a bi-national scientific collaboration between Mexico and the USA, led by the Instituto Nacional de Astrofísica, Óptica y Electrónica (INAOE) and the University of Massachusetts at Amherst. The telescope currently operates at wavelengths from 4mm to 1mm, and during the dry winter months the LMT site provides the highest levels of atmospheric transmission and potential future access to submillimeter observing windows. This paper describes the current status and scientific performance of the LMT, the suite of scientific instrumentation and future engineering upgrades that will optimize the optical efficiency of the telescope and increase its scientific productivity.

Keywords: mm-wavelength, camera, kinetic inductance detector, Large Millimeter Telescope

1. OVERVIEW

The Large Millimeter Telescope (LMT) is a 50m-diameter millimeter-wave radio-telescope designed to operate with good optical efficiency at wavelengths between 4mm and 1mm. Under optimal atmospheric conditions the LMT is capable of conducting future observations in the 0.8mm atmospheric window. The telescope optics deliver a field-of-view of 4 arcmins (diameter) and can point to astronomical sources with an accuracy $\lesssim 1$ arcsec RMS. The large aperture and collecting area of the primary reflector provide angular resolutions (4 - 18 arcsecs) which, when combined with the mapping speeds of the LMT large-format ($\sim$kilo-pixel) continuum cameras and multi-pixel heterodyne arrays, will complement the capabilities of the current (sub-)mm ground-based interferometers and single-dish lower-frequency radio telescopes. The LMT represents an important binational federally-funded science project undertaken by Mexico and the United States, and led by the Instituto Nacional de Astrofísica, Óptica y Electrónica (INAOE) and the University of Massachusetts Amherst (UMASS) respectively. Furthermore as the largest single-dish millimeter-wavelength telescope already constructed and operating at a wavelength of

Send correspondence to D.H. Hughes:
Email: dhughes@inaoep.mx

Ground-based and Airborne Telescopes VIII, edited by Heather K. Marshall, Jason Spyromilio, Tomonori Usuda, Proc. of SPIE Vol. 11445, 1144522 · © 2020 SPIE
CCC code: 0277-786X/20/$21 · doi: 10.1117/12.2561893

1mm (and with the ability to also deliver future submillimeter astronomical observations), the LMT provides new and unique research opportunities that will contribute to the continuous international development of major multi-wavelength (gamma-ray to low-frequency radio) ground-based and space-borne astronomical facilities to explore and understand the physical nature of our Universe.

The LMT is an "open-air" telescope, designed by MT Mechatronics (formerly MAN) with no radome or astrodome enclosure to obstruct its view (Figure 1). This configuration provides optimum performance under the best observing conditions, particularly for measurements with sensitive, broadband continuum systems. The 50-meter diameter primary reflector consists of a total of 180 individual surface segments distributed in 5 concentric rings. Each segment is connected by 4 actuators to the steel truss of the antenna backup structure. Gravitational deformations of the primary reflector and environmental effects such as temperature gradients within the telescope steel structure and wind loads, all pose significant problems to achieve the specification of 75 microns RMS for the total optical error budget derived from surface accuracies of the principal telescope optics, and to achieve the sub-arcsecond offset-pointing requirements of the LMT. The original design approach was therefore to combine a homologous telescope construction with an active control system to continuously update the positions of the individual surface segments, and hence correct the effects of these deformations and maintain the optimal global shape of the 50-m diameter primary reflector during scientific observations. Experience has shown that under night-time (thermally-stable) and low wind conditions, the active control of the primary reflector provides constant gain from the telescope optics as the LMT tracks and observes sources over the nominal range of telescope elevations (20 to 80 degrees). Future engineering projects will continue to improve the ability of the active surface control system to correct the thermal deformations which will then provide even greater aperture efficiency, particularly at the highest frequencies, and enable day-time observing to increase the scientific productivity of the LMT.

1.1 LMT site infrastructure

The LMT is supported on foundations that include a large basement area for site-related activities. The space is divided to include an on-site warehouse for spares and equipment, kitchen, showers and bathrooms, offices and laboratories that can be customized to support the delivery and preparation of major hardware and instrumentation before their installation and integration into the LMT engineering systems. In the near future it is expected that some of these spaces in the LMT basement will be adapted to create working and sleeping/resting areas that can be supplemented with additional oxygen to lower the effective altitude of these enclosed spaces from 4600m to approximately 2600 – 3000m. When complete, these modified areas will then allow LMT staff and visiting scientists to operate the telescope under more comfortable conditions and safely spend working shifts and periods of multiple days at the site without the need to travel to and from the LMT basecamp, which is located in Ciudad Serdán (altitude 2500m), approximately a 1 hour drive (45 km) from the LMT site.

The LMT has a 25-m high tower structure attached to the alidade that rotates with the telescope in azimuth. This tower contains 3 additional levels of working areas that house the electrical power switches, transformers and drive control cabinets for the major electromechanical systems (azimuth and elevation drives, tertiary mirror gear motors, secondary mirror hexapod, primary reflector actuators). The tower also houses the telescope control room for scientific operations, the instrumentation back-end room for the racks of warm-electronics systems for each scientific instrument and other engineering systems, and a large 100 sq. meter receiver room that can accommodate all of the front-ends of the various spectroscopic receivers and continuum imaging cameras, their warm coupling optics and cryogenic compressors.

The LMT tower structure, antenna alidade, and primary reflector backup structure are enclosed by thermal cladding, as specified by the original design. The cladding protects the structure from direct exposure to sunlight, slowing the structural response to the daily thermal warming cycle.

Additional external site infrastructure includes an electrical substation that receives power from the Mexican federally-operated electrical distribution network. The LMT electrical substation houses a primary 750 kVA transformer that delivers all the necessary electrical power during normal scientific, engineering and maintenance operations. The substation has a backup transformer of equal capacity, and a smaller 350 kVA transformer for non-essential services. In the event of a total loss of electrical power delivered to the summit site, the LMT can continue to operate with two emergency automatic start-up diesel generators with a primary 1000 kVA generator,

Figure 1. (Above) The 50-meter diameter Large Millimeter Telescope showing the primary reflector containing 180 high-precision surface segments distributed in 5 concentric rings (with 12, 24, 48, 48 and 48 segments respectively). The inner 32-m diameter (rings 1 to 3) of the primary reflector is located interior to the tetrapod legs (in ring 4) that support the 2.7m secondary mirror and hexapod. (Below) The rear-view of the telescope reflector, the ballast cantilevers and the 25-m high building (tower) that contains the elevator to access the drive control units for the major electro-mechanical systems, the telescope control room, and the receiver back-end rooms and main receiver cabin for the scientific instruments. All of telescope structure is enclosed in thermal cladding. The concrete ramp that leads down into the telescope basement, providing access to the telescope, can be seen in the foreground.

and a backup 350 kVA generator that can power the Emergency Elevation Drive Cabinet and safely move the telescope in elevation to its secure stow position under any emergency situation. The LMT site and the telescope is protected from lightning strikes by 4 lightning towers around the summit site perimeter (Figure 2), a lightning rod installed on the primary reflector and an additional lightning rod on the head of the tetrapod. A 64-m high tower-crane provides access and maintenance of the primary and secondary reflectors. The tower-crane is also used to enable photogrammetry measurements of the primary reflector at different elevation angles. The summit site has a small metrology hut that allows the alignment precision of the primary surface segments to be measured with laser-trackers after their delivery to the site, and to make any final iterative adjustments of the position of individual panels prior to the final installation of segments into the reflector.

Figure 2. Aerial view (late afternoon) of the summit of Volcán Sierra Negra (altitude 4600m). The site shows the LMT pointing north. The electrical substation, workshop and metrology building can be seen to the left of the telescope, and above the ramp. The green tower-crane (in its lowered position) provides access for installation and maintenance to the secondary mirror, hexapod and segments of the primary reflector (M1), as well as providing the platform to conduct photogrammetry measurements of M1. The red building is occasionally used as a visitor center, and the meteorological equipment including the 225GHz radiometer and external cameras are installed on the roof area of this building. Multiple lightening protection towers are distributed around the summit site.

1.2 LMT site and meteorological conditions

The LMT is situated on Volcán Sierra Negra (18d 59m 08s N, 97d 18m 53s W) at an altitude of 4600m. The telescope site is easily accessible with a 2.5 hour drive (∼120km) from the INAOE campus in Tonantzintla (at an altitude of ∼2200m) that serves as the operational headquarters in Mexico.

The LMT site was selected in 1997 following radiometric testing at a number of potential high mountain sites in Mexico. The location of the LMT at a northern latitude of +19 degrees also provides very good coverage of the southern sky, with the Galactic center culminating at an elevation of about 45 degrees, and delivers access to sources in the southern sky down to declinations of approximately −50 degrees. The latitude of the LMT site is identical to the Mauna Kea Observatory in Hawaii and provides approximately 70% coverage of the sky that can be seen by ALMA. The LMT provides many opportunities for collaborative projects that require simultaneous observations or follow-up observations of astronomical sources that are targeted by the major multi-wavelength observatories in both hemispheres.

The high altitude of the LMT site provides high millimeter-wavelength atmospheric transmission. Given the tropical latitude, the summer months have extended periods of higher humidity and increased cloud cover so that

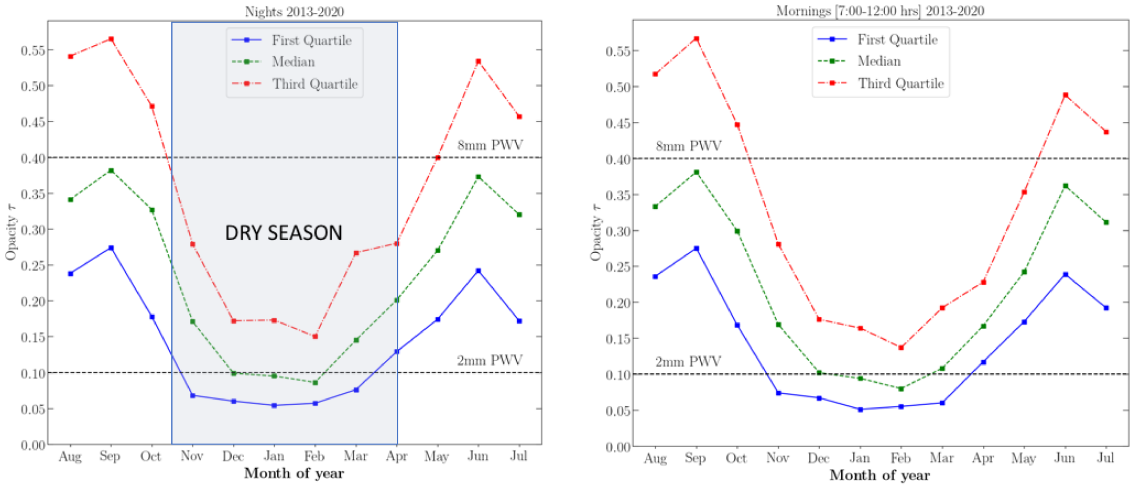

Figure 3. Monthly-averaged opacities derived from 225 GHz radiometer measurements at the LMT over the period of 2013-2020. The first, second (median) and third quartiles of the opacity data are shown for night-time (dusk to dawn) observing, and also for a 5 hour period after sunrise that demonstrates the opportunities for daytime observing. The site allows for 3mm operation throughout the year, while 1mm wavelength operation is optimized during the period October through May. During the less frequent periods of good weather during the summer, 1mm measurements are still possible within a flexibly-scheduled allocation of telescope time that maximizes the opportunities to observe at the highest frequencies.

the best high frequency (> 200 GHz) observing conditions typically occur during the winter and spring months. The sky transmission is continuously measured, with a recorded sample every minute, at 225 GHz (1.3mm) using a tipping radiometer. Figure 3 shows the night-time opacity statistics for the radiometer data obtained during the period 2013-2020. From November through April, the LMT site has a median atmospheric opacity at 1.3mm lower than 0.2 while the first quartile opacity typically falls below 0.1 (zenith transmission at 1.1mm $> 90\%$). The site also offers extremely good submillimeter observing conditions with an opacity less than 0.06 for a few hundred hours per year in the same period.[1] During the summer months the site is still good enough for observations in the 3mm and 2mm windows, interspersed with shorter unpredictable periods of access to the 1mm window. It is common to have electrical storms and local cloud-cover (and hence the risk of snow and formation of ice on the telescope structure) over the site during the afternoons in the summer months of July and August. Depending on the severity of these summer weather conditions, the radiometer may be powered off to prevent any damage when scientific observations are cancelled. Consequently the monthly statistics of the opacity data in these summer months can be biased by the quantity of the data collected, and the year-to-year variations in the summer weather conditions.

It is important to note that the opacity data also demonstrate that extended daytime observations are feasible, particularly during the winter and spring seasons.[1] This provides the motivation to develop and implement engineering upgrades to reduce the measured thermal gradients within the telescope steel structure, and to provide more precise active control and correction of the thermally-induced deformations of the primary reflector, thereby improving the overall telescope performance to allow daytime observations.[2]

The meteorological data show that the weather conditions are generally benign for such a high-altitude site and hence are favorable to the operation of a large antenna. There is only a small seasonal variation of the daily median temperature (< 1 deg. C) and the diurnal temperature cycle is small (< 5 deg. C). The median wind speed at the site is < 5 m/s. Sub-arcsec offset pointing is possible for 90% of the time when wind-speeds are below the LMT design specification of 10 m/s. The LMT typically continues to observe until wind speeds exceed a limit of 15 m/s. The maximum operational wind-speed for the LMT is 25m/s, at which point the telescope moves to a secure stow position with the primary reflector locked at an elevation of 10 degrees.

2. TELESCOPE OPTICS

2.1 Primary reflector

The 50-meter diameter primary reflector of the LMT is constructed from a steel truss that supports 180 individual reflector segments arranged in five concentric annular rings, with 12, 24, 48, 48 and 48 segments in rings 1 to 5 respectively (Figure 1). Each segment measures approximately 5 x 3-m and provides the supporting structure for the reflective surface panels. In 2005 the project committed to a design concept of using precision composite electroformed nickel panels (with a rhodium coating) built by Media Lario Technologies, the Italian company responsible for fabricating the reflector surface in the European ALMA antennas. Individual panels were delivered to the LMT project with an RMS surface error of 15 microns or better.

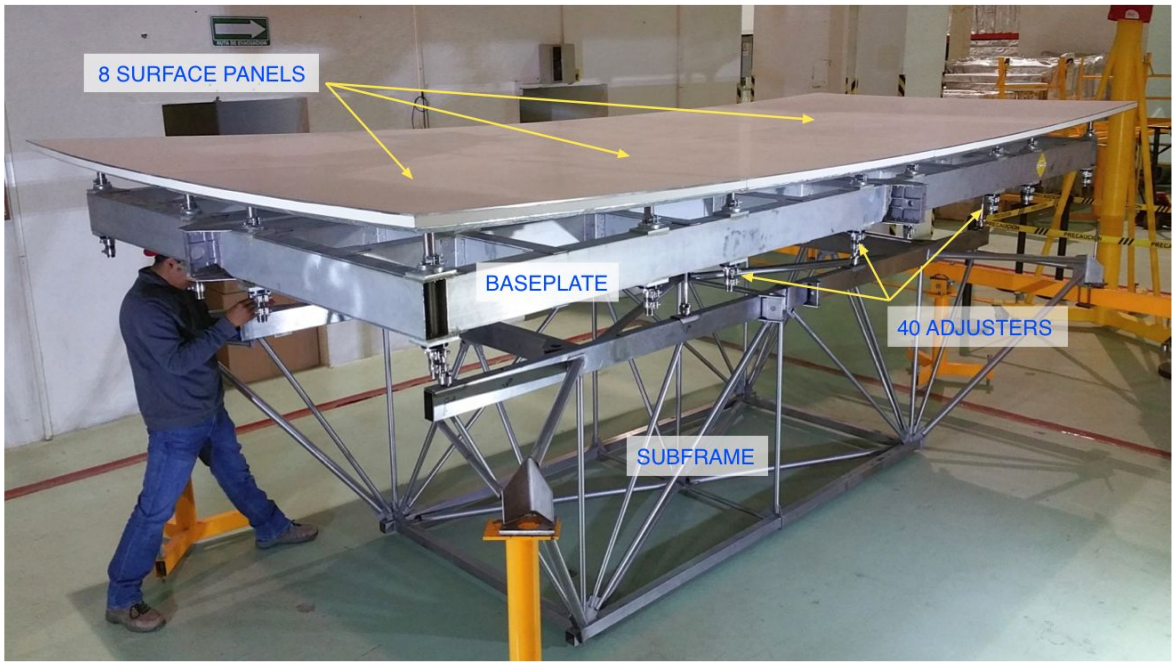

Figure 4. A primary surface segment following assembly and alignment at the INAOE Aspheric Surfaces Laboratory in Puebla. 8 surface panels are supported on an aluminum box-construction baseplate, attached by five mechanical adjusters per panel. The assembly is attached to a stainless steel subframe that provide stiffness, and facilitates mounting on the antenna back structure at the four corner points visible in the figure.

The major components of the reflector segments are shown in Figure 4. Each segment is supported by a stainless-steel subframe truss that is attached to the antenna truss structure by 4 actuators for axial support and motion, and 3 lateral bars for lateral rigidity. The subframe connects to an aluminium base-plate via 8 slender stainless-steel axial bars. As with the subframe, the base-plate is connected to the steel truss by a separate set of lateral bars. The reflecting surface of a segment consists of 8 Media Lario panels, each attached to the baseplate by 5 mechanical adjusters.

Thermal insulation is applied to the underside of the panels to reduce any thermal gradients across the aluminium base-plate to <0.1 deg C. The surface of an individual segment is set to its correct parabolic shape by modifying the heights of the 40 panel adjusters. The iterative adjustment process is carried out using a commercial laser tracker following segment assembly.

Each segment contains multiple mechanical components that must work together to produce the required individual surface-segment accuracy and stability. A review of the design and manufacture of segment components, together with improved metrology and integration techniques, has allowed the project to continuously reduce the typical alignment errors in the individual segments. Figure 5 shows the evolution of the average RMS surface-error of the segments within each ring segment of the primary reflector. The typical precision of the most

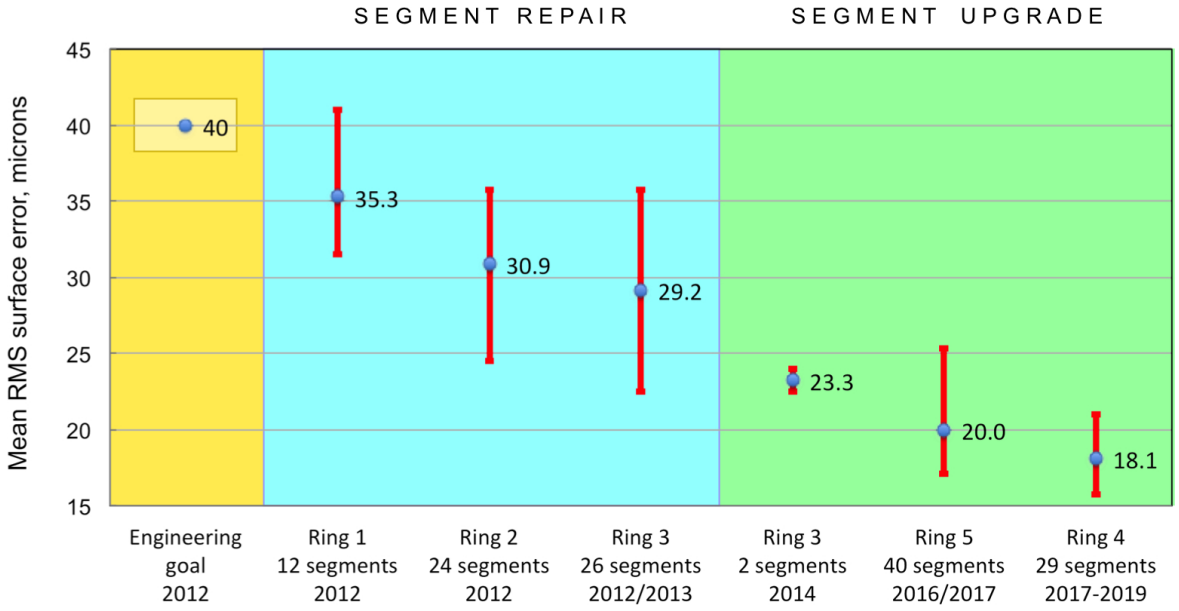

Figure 5. Evolution of the mean RMS segment surface error following technical reviews carried out in 2012. On-site segment repair activities on the inner three rings in 2012-13 led to the development of a segment upgrade process, first trialled on two ring 3 segments in 2014. The upgrade program was applied during ring 5 assembly, and is presently being carried out for all segments in ring 4.

recent segments installed into the outer two rings of the 50-meter diameter primary reflector is 20 microns RMS or better, comparable to the precision of the segmented secondary mirror (see section 2.2).

A number of performance issues still need to be addressed for a subset of 11 segments in ring 4 (that were originally installed with lower-quality panels provided by another supplier, and will be substituted for the Media Lario panels). Furthermore it will be possible, without any technical or engineering risk, to improve the alignment accuracy of segments in the inner three rings, where many are known to have surface errors of 30-40 microns RMS. The goal of the segment maintenance program is to maximize the aperture efficiency of the primary reflector, particularly at the highest frequencies, by reducing the contribution of the precision of the individual segments to the overall optical error budget, and leave the residual un-corrected environmental effects (gravitational and thermal distortions, and the impact of wind) as the dominant factors that place a limit on the performance of the telescope.

In addition to the segment upgrade program mentioned above, which advances steadily during a normal observing season without interrupting the science program, individual surface panels are routinely inspected for damage (by falling ice for example), and are replaced with spares if damage or delamination of the panel is severe.

All global alignment activities on the LMT-50m are carried out using photogrammetry to measure the reflector surface.[3] Photogrammetry does not require access to the prime focus, and hence can be carried out with minimal disruption to the observing schedule. A single photogrammetry map is obtained by taking approximately 200 individual camera images, using the site tower crane to position the camera. This requires around 30 minutes of camera time, plus 10 minutes to process the data and extract the surface point cloud. Since the tower crane is lowered during the winter months, mapping of the primary reflector can only be conducted from April through December each year.

2.2 Secondary mirror & hexapod positioner

In 2016 the project took delivery of a new secondary reflector, since the original monolithic aluminium reflector was not compatible with the full 50-meter primary aperture. Media Lario Technologies of Italy were contracted to build a 2.7 meter segmented reflector using the same Rhodium-coated Nickel composite-panel technology

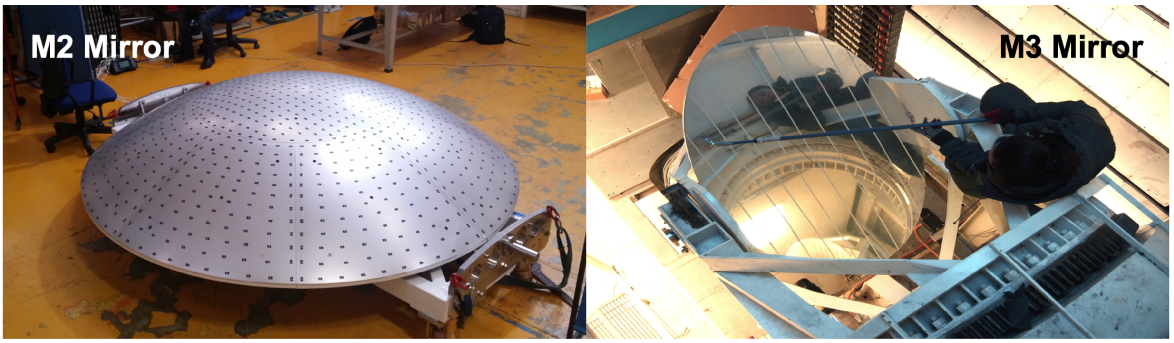

Figure 6. (left) The segmented secondary reflector during a project metrology review at the Media Lario manufacturing facility in Italy, 2016. The reflector, comprising a 1.2-m diameter central panel surrounded by 8 petals, is mounted on a rotatable carriage designed to permit surface measurements at multiple elevations and facilitate reflector installation on the telescope. Temporary photogrammetry targets are clearly visible. (right) The tertiary mirror seen looking down into the receiver room from the apex cabin. A laser tracker is being used to measure mirror flatness. The elevation tracking gear of the mirror positioner is visible lower-right

employed for the primary surface panels.[4] The reflector is composed of a central circular panel of 1.2-m diameter (that illuminates the inner 32-m of the primary reflector), surrounded by eight identical petals (Figure 6 - left panel). The panels are mounted on a painted stainless-steel truss back structure using five adjusters per panel. Unlike the primary panels, the secondary panel adjusters are accessed from the front-facing panel surface, similar to the design of the ALMA panels. The complete assembly was mounted and aligned at Media Lario´s production facility in Italy, and then shipped to the LMT site with no loss of surface accuracy. More details of the design and manufacture of the secondary reflector are described elsewhere.[4] The use of Media Lario´s composite panel technology provided the benefits of reduced weight (around 210 kg) and a measured RMS surface error of 25 microns at 60 degrees elevation. While the current RMS error is dominated by the central panel, the project has also purchased a higher-quality spare central panel from Media Lario that has an RMS error of just 8.5 microns.

A new hexapod positioner for the secondary mirror was provided by Symetrie of Nimes, France. Calibration tests of the hexpod yielded excellent results, with calibrated errors of less than 5 microns in the translation degrees of freedom and less than 1 arcsec in the rotations.[5] The new hexapod was installed, along with the new M2 mirror, in the Fall of 2017 in advance of the LMT/GTM's first observing season as a 50m telescope.

2.3 Tertiary mirror & positioner

The LMT is a bent Cassegrain optical design. The flat M3 mirror, shown in figure 6 (right panel), accurately tracks the primary reflector as it moves in elevation and directs the beam along the elevation axis to the Cassegrain focal point. The tertiary mirror maintains alignment between the telescope optics and the instrument optics, since the latter is elevation invariant. Located approximately 7 meters behind the apex of the primary reflector, the tertiary mirror is a machined aluminium flat with an elliptical outline whose major and minor axes measure 1.7 and 1.1-m respectively. Unlike other LMT optics, the tertiary reflector is highly polished, which assists with system alignment during the installation of new instruments. The tertiary mirror, which weighs 98kg, is mounted on a positioner using five mechanical adjusters that facilitate fine angular-positioning of the reflector following installation, and also some adjustment of the final surface flatness error. The tertiary mirror was aligned in 2015 and currently has an RMS flatness error of 39.5 microns. The tertiary positioner provides tracking in elevation, seamlessly synchronized with the antenna control unit (ACU). The positioner direction is switched manually to rotate the detector beam paths by 180° along the elevation axis before coupling to the different sets of instruments mounted in the left and right halves of the instrument cabin.

3. TELESCOPE CONTROL SYSTEM

The LMT azimuth drive system is a wheel-on-track mechanism that carries the vertical loads of the telescope with sixteen individually-driven wheels on a 39.6-m diameter circular track. The track is welded from high strength steel to provide a continuous top surface and is levelled to 175 microns RMS to facilitate smooth

tracking. The LMT main reflector is attached to the alidade structure via two elevation bearings and is driven by the elevation drive system which consists of two 11-m diameter circular gear rims with their centers at the elevation axis, each driven by two pinions supported by a carriage. All twenty of the drives (sixteen in azimuth and four in elevation) consist of a motor, gearbox and brakes. These drives are controlled by a fully digital servo system that is divided into a drive control unit which consists of the servo amplifiers and an embedded PLC that implements torque sharing and safety interlocks, and an antenna control unit that implements the servo control loops and astronomical tracking. When the LMT is required to be securely stowed, and not parked (using the brakes), for example due to adverse weather conditions or after completing scientific observations, the telescope is moved to an elevation of 10 degrees and two stow pins are inserted between the A-frame of the alidade and the ballast cantilever of the reflector. Since stowing the telescope during the worst weather conditions is critical to its survival, an elevation axis emergency drive control unit (EEDC) backups up the main drive control unit to manually drive the telescope to its stow position.

The LMT Control System was developed at UMass and has been in use at the LMT since 2008 enabling routine operations in support of both engineering and scientific tasks. The Monitor and Control Systems software consists of three major elements: (1) the software framework, within which the LMT applications are written; (2) the Telescope Control System (TCS), which runs the telescope and all subsystems, including the active-surface control system of the actuators primary reflector; and (3) the Data Collection System (DCS), which coordinates the functions of the telescope and instruments to take and record scientific data.[6,7] The real-time data logging and display capabilities of the LMT monitor and control system have proven to be extremely effective and important in tuning and optimizing the performance of the telescope drive systems.

Further details on the architecture and tracking performance of the telescope control system, with a range of tracking speeds between less than sidereal rates up to 0.1 degs/sec, have been published previously.[8,9]

4. TELESCOPE UPGRADE HISTORY AND CURRENT PERFORMANCE

Since the LMT first-light observations were conducted at 3mm and 1.1mm in the spring 2011, with the Redshift Search Receiver and AzTEC respectively, and using only the inner 32-m diameter of the primary reflector, the optical performance of the telescope and its operational efficiency have continued to improve. We describe the engineering path to achieving the current performance and some of the major milestones. Two of the most significant influences on the increase in telescope sensitivity have been the expansion of the diameter of the primary reflector from 32m to 50m, and the improvement in the surface alignment precision of the individual surface segments. In this section we hereafter refer to these telescope configurations with different primary reflector diameters as the LMT-32m and the LMT-50m respectively.

4.1 LMT-32m first-light and passive alignment of primary reflector

The LMT-32m first-light observations successfully demonstrated the full functionality of the mechanical drive systems and telescope optics, as well as the antenna control software and the first-light scientific instruments. However these initial end-to-end tests identified concerns with the overall telescope performance and optical efficiency. Although these first observations of molecular gas and dust in local and high-redshift star forming galaxies showed clear detections, with comparable quality and signal-to-noise to those previously obtained with smaller diameter (10-15m) submm and mm telescopes, it was immediately clear that the LMT-32m sensitivity was not as high as expected.

In mid-August 2011 a new LMT management and administrative team launched a comprehensive series of technical reviews and engineering studies to identify the cause of the reduced telescope performance, and to recommend solutions. It was concluded that the primary cause of the reduced sensitivity was dominated by quality-control issues during the earlier integration and alignment of the individual surface segments installed in the inner 3 concentric rings of the primary reflector. Other contributing factors included the performance of the original active-surface control system, in particular the first generation (year 2006) of electro-mechanical actuators, and the surface precision and shape of the machined aluminium secondary mirror compared to the original design specifications.

Throughout 2012 and 2013 an intensive engineering program addressed the most critical problems and upgraded the performance of the primary surface segments, their actuators and electronic control system. The main

activities included the systematic removal, repair and modification to the surface segments and actuators in the inner 3 rings by the LMT engineering groups at INAOE and UMASS, with additional support from MERLAB (Georgia, USA).

Initially an extensive set of repairs to 62 of the 84 primary surface segments of the LMT-32m was conducted by the INAOE engineering group at the LMT site. These repairs required the removal of the segments from the antenna backup structure, followed by the partial disassembly and reintegration of reflector panel support components (approximately 2500 per segment), including replacement of damaged or defective components where necessary. The immediate increase in optical performance of the re-constructed segments was dominated by greater enforcement of quality control processes and management of the mechanical and engineering activities, improvements to the stability and strength of the flange connection between the electroformed nickel panels and their adjusters, and investment in new metrology equipment to allow the use of portable laser trackers (compared to a CMM). The binational LMT metrology team also developed new software analysis code, and implemented new procedures to align the 8 reflective panels within an individual surface segment. As a result of this effort the majority (80%) of the segments in the inner 3 rings had significantly improved alignment precision in the range of 25 – 40 microns RMS by the end of 2013 (Figure 5).

Following the reinstallation of the upgraded segments into the inner 3 rings of the primary reflector, metrology measurements were made with holographic observations at 12 GHz using geo-stationary satellites at elevations of 61 degrees to globally align the inner 84 segments. As a result the LMT-32m had a competitive primary aperture efficiency and sensitivity for scientific observations at 3mm. However since the electro-mechanical actuators were still undergoing a series of modifications and upgrades, and a new active surface control system was under development, the surface segments were connected to the backup structure using simple threaded rods. Consequently the global surface alignment of the reflector segments in early 2013 was iteratively improved by making manual adjustments to these connecting rods whilst the telescope was pointed to zenith, with a compensation to provide a maximum antenna gain at an elevation angle of 60 degrees. This passive primary surface of the LMT-32m had a restricted elevation-range about its alignment elevation angle ($\pm 35^\circ$ at 3mm, $\pm 10^\circ$ at 1mm) over which the telescope could be used to conduct astronomical observations, due to the strong influence of elevation-dependent gravitational deformations. It was possible however to conduct a brief Early-Science shared-risk science program in 2013 and obtain valuable information regarding the telescope pointing performance, and variation in gain of the primary surface as a function of elevation without the installation of the active-surface control system.

4.2 LMT-32m with active alignment of primary reflector (2014 - 2018)

The next major milestone towards the goal of achieving the original design specifications of the telescope was the installation and implementation of a new active surface control system that could provide full and continuous correction of the position of the individual primary reflector surface segments, and maintain the global alignment as the telescope slewed and tracked astronomical sources over the full range of accessible elevations (20-85 degrees). The installation of a functioning (though not yet optimal) electromechanical actuator network[10,11] in rings 1-3 paved the way for the development of a new active surface setting algorithm. Using the holography measurement technique described, it was now feasible to measure the surface shape for a series of telescope elevations, and to optimize the surface precision at each elevation by adjusting the actuators and the positions of the individual segments. The location of geosynchronous satellites observed from the LMT site provided holography maps for elevations of 43, 52, 62 and 68 degrees. Since night-time holography maps taken hours apart showed systematic deformations in the shape of the primary reflector, due to thermal gradients within the telescope steel structure, it was necessary to first remove these effects from the maps. The main thermal distortion produces a vertical astigmatism in the primary reflector. It became possible to solve for this effect, and remove this distortion using the active-surface control system, by taking regular measurements of the antenna gain and beam pattern during the night.[12] Due to the limited elevation range, a linear model was used to represent the best actuator position as a function of elevation angle. The implementation of this model in the active surface control system demonstrated its effectiveness to deliver near-constant antenna gain ($\pm 5\%$) over the full elevation range of the LMT-32m (see Figure 7).

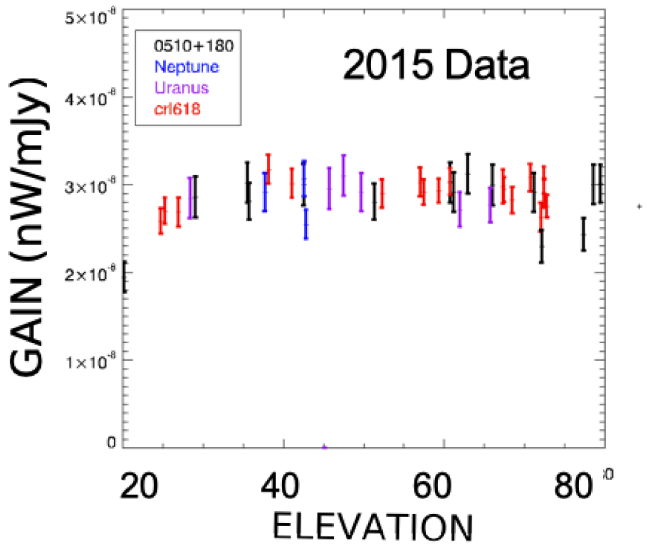

Figure 7. Measurements of the antenna gain at different elevations made at a wavelength of 1.1mm by the AzTEC instrument in 2015. The active surface of the LMT maintains a near-constant value of the gain over its an elevation range from 20-85 degrees.

In addition to the improvement in the precision alignment of the individual segments and their active positional control, the optical performance of the LMT-32m also benefited from the first applications of photogrammetry as the metrology technique to accurately measure the location of the individual segments within the inner 3 rings. A detailed description of the photogrammetry technique and results is provided in Gale *et al.*[3] Each reflector segment has 32 photogrammetry targets located close to the individual reflector panel corners. The three-dimensional point cloud of the positions of all targets produced by the photogrammetry camera is fit to a best parabola and, for each segment, the resultant residuals are used to determine the optimum alignment settings for the four actuators attached to that particular segment. Photogrammetry measurements are carried out at night to minimize the changes in the surface shape due to thermal deformations. An advantage of photogrammetry is that it enables the measurement of the global deformations of the primary reflector over a larger range of elevation angles, unconstrained by the limited positions of geo-stationary satellites during the earlier 12 GHz holography measurements. This significantly improved the ability to understand the large-scale gravitational deformations of the primary reflector under normal operational conditions. Consequently photogrammetry yielded excellent results and delivered competitive scientific performance for the LMT-32m with a total error budget for the telescope optics equivalent to 85 microns RMS (see Figure 8).

4.3 LMT-50m with active surface control (2018 – current)

As described previously, mechanical and software engineering solutions were successfully implemented to optimize the alignment precision of the individual primary reflector segments, and actively control the global alignment of the primary reflector of the LMT-32m under normal operational conditions. This work continued as our understanding of the behavior of the telescope optics, particularly in response to the influence of thermal gradients in the telescope structure, improved.

Since 2016 there have been four significant engineering efforts that have further increased the scientific performance of the LMT. The design and construction of the new secondary mirror and its hexapod positioner have already been described in §2.2. The most visible of these projects was the expansion of the diameter of the primary reflector from 32-m to its final specification of 50-m. This required the fabrication of an additional 768 electroformed-nickel panels (plus spares) by Media Lario Technologies according to the original design specifications, followed by the integration and alignment (in the Aspherics Laboratory at INAOE) of 96 surface segments that were installed in the outer two rings of the primary reflector. The earlier segment repair work for the 32-m

surface led to the redesign of key panel adjuster components, and improved quality control in their manufacture. The segment integration process also benefited from new procedures, including alignment of the mechanical structure using laser trackers. The resulting upgrades to segment manufacture were successfully trialed on two ring 3 segments in 2014 before being rolled out for rings 5 and 4 from 2016. The upgrade program enabled a further reduction in segment surface error to just below 20 microns RMS for the period 2017-2019 (Figure 5).

Together with the production of the additional surface segments, it was also necessary to expand the active-surface control system and more double the number of actuators. A number of different actuator designs have been employed on the LMT over the years, both in terms of hardware and control electronics. The most recent (and most successful) deployment uses electro-mechanical actuators designed and manufactured by ADS International S.R.L of Italy.[13,14] The actuators use a rotating pre-loaded (zero backlash) M16 screw-nut assembly with precision stepper gear-motor. A total of 384 ADS actuators have been installed for active control of outer rings 4 and 5. Actuator installation was completed in mid-2018 shortly after the last ring 5 segments were installed in the primary reflector. The eventual goal is to replace all of the first-generation actuators in rings 1-3 with the improved ADS design.

Following the conclusion of the integration of the full 50-m diameter primary reflector and its active surface control system, together with the upgraded M2 mirror and hexapod, in mid-2018 it was possible to begin the engineering and scientific commissioning activities of the LMT-50m.

4.4 Current Antenna Performance

In this section we summarize the current performance of the Large Millimeter Telescope. There are two basic parameters to be considered: (1) the effective area (or gain) of the antenna; and (2) the ability of the antenna to point accurately.

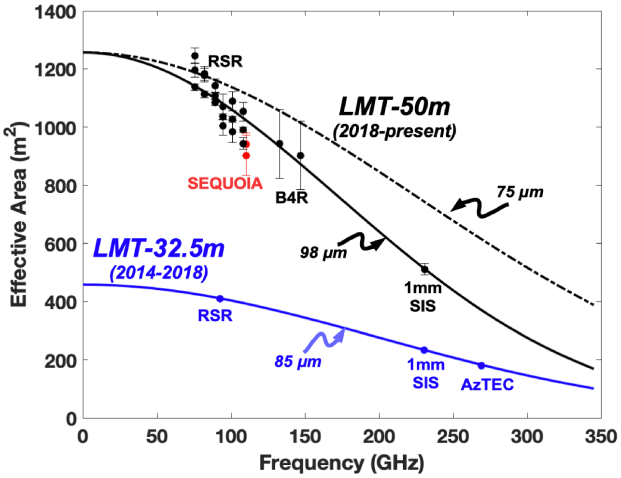

Frequency (GHz)	Aperture Efficiency	Main Beam Efficiency	Gain (Jy/K)
85	0.58	0.68	2.42
100	0.55	0.65	2.56
115	0.52	0.61	2.70
140	0.47	0.55	2.99
230	0.27	0.31	5.21

Figure 8. (left) Effective area of the LMT as a function of frequency. The curve in blue summarizes effective area measurements with the 32.5m LMT surface. The variation in gain with frequency is well described by an overall RMS of 86 microns. The curves in black are for observations made with the 50m LMT. The difference in effective area with the completion of the antenna is obvious. The effective area of the 50m antenna is well characterized by an overall surface RMS of 98 microns. Also shown (dashed line) is the predicted improvement that should occur as the antenna surface is improved to 75 microns RMS. (right) Summary table of current LMT-50m aperture efficiency, main beam efficiency and antenna gain.

4.4.1 Antenna Effective Area

The effective area of an antenna measures the amount of power that the antenna collects from astronomical sources. The effective area is always less than the geometrical area of the 50m aperture for a number of reasons: (1) the illumination of the antenna surface by the receiver feed; (2) blockage of the aperture by the secondary mirror and its supports; and (3) shadowing of the incoming beam by the secondary mirror supports. In addition,

for the LMT, the eight segments at the base of each subreflector support, which are significantly blocked and shadowed, have much lower surface accuracy and do not contribute much to the total LMT signal. Putting all of the above effects together predicts that approximately 69% of the 50m-aperture will contribute to the observed signals.

In addition to the above effects, departures of the reflector surface from its nominal parabolic shape will lead to a decrease in the signal which will depend on the wavelength of the observed signal. This behavior is well described by a relation derived by Ruze.[15] Let $A_E(\nu)$ be the effective area of the antenna as a function of frequency, then

$$A_E(\nu) \;=\; A_E(0)e^{-\left(\frac{4\pi\nu}{c}\epsilon\right)^2} \tag{1}$$

The Ruze equation has two parameters: the RMS surface error (ϵ) and the intercept value of the effective area at zero frequency ($A_E(0)$). Figure 8 shows effective area measurements for the LMT-32m configuration and the LMT-50m configuration. The measurements for the LMT-32m configuration are consistent with an overall surface RMS of 85 microns, as described in previous sections. The measurements of the LMT-50m configuration show the obvious expected increase in the effective area with the completion of the full reflector surface. The data are consistent with an overall optical RMS of 98 microns and a zero-frequency intercept of 64%. This latter value is somewhat low compared to the expected value of 69%, though this may be within measurement errors.

The difference between the overall RMS error in the LMT 50m (98 μm) and that of the LMT 32.5m (85 μm) is notable and a matter of active investigation. The present understanding of this situation is that thermal deformations of the LMT surface have a greater effect on the setting of the 50m surface than were apparent in the 32.5m-diameter surface. Photogrammetry measurements of the surface during the night demonstrate that even during night time conditions, when the measurements are made, there are significant changes that are related to temperature gradients within the antenna backup structure.[2] Therefore, simple iteration of measurement and setting of the surface did not converge to a good result because the surface changes from map to map. A new scheme which accounts for low spatial order thermal deformations is under development to improve the surface setting.

4.4.2 Antenna Pointing

Pointing a large antenna accurately is a major technical challenge. Two metrics for pointing a large antenna may be defined: (1) the absolute pointing, which refers to the antenna's ability to point blind at any point on the sky; and (2) the relative (or offset) pointing, which refers to the antenna's ability to point to a position after peaking up on a nearby pointing calibrator source.

Figure 9 illustrates the results of a measurement of the absolute, all sky, pointing model. Five nights of pointing measurements were obtained with the sky sampling shown in the left panel of the figure. The model fit makes use of a standard pointing model following Stumpff[16] with an allowance for pointing drifts from night-to-night. The overall fit to the data yields an RMS of approximately 2 arcseconds in each coordinate.

For scientific observations, the LMT does not rely on the absolute pointing accuracy to acquire a scientific target source. Measurements are typically made on a nearby pointing calibration source to resolve pointing drifts during the night due to thermal deformation of the antenna. With a nearby pointing check, the relative pointing area on target sources is $\lesssim$1 arcsecond.

5. SCIENTIFIC INSTRUMENTS

The LMT is outfitted with a suite of scientific instruments covering the atmospheric windows between 3mm (90 GHz) and 1.1mm (280 GHz) and including both spectroscopic and continuum imaging capability. In this section we describe our current suite of facility-class instruments and two new instruments expected in 2021. A 2mm single-beam dual polarization heterodyne receiver, B4R, based on an ALMA band-4 mixer, has recently been installed and commissioned. Details of this guest instrument will be described elsewhere.

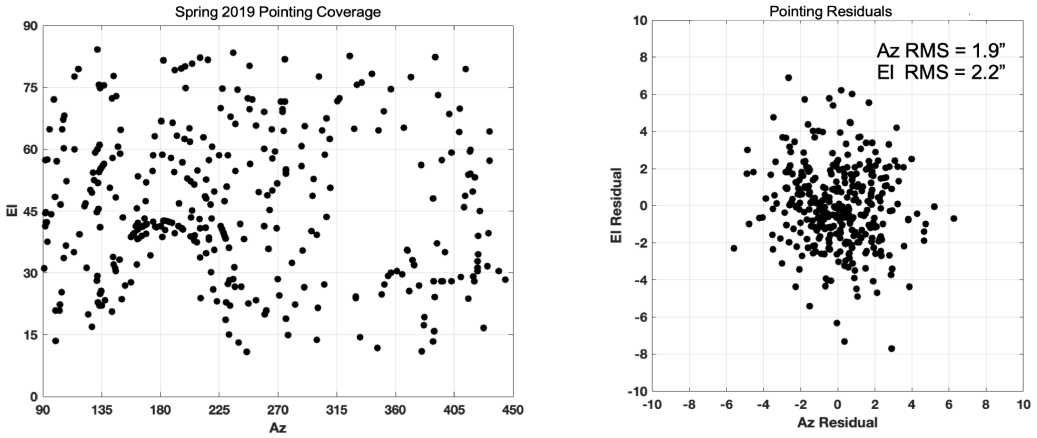

Figure 9. Pointing measurements made on five consecutive nights during the spring of 2019 with the SEQUOIA instrument. The left panel shows the all sky pointing coverage for the experiment. The right panel shows the residuals to the pointing model fit.

5.1 The Redshift Search Receiver

The Redshift Search Receiver (RSR) is a novel MMIC-based receiver[17] designed to maximize the instantaneous receiver bandwidth to cover the 3mm wavelength atmospheric window (73 – 111 GHz) in a single tuning. The receiver has four pixels arranged in a dual-beam, dual polarized configuration (see Figures 10 and 11). Orthogonal polarizations are combined in waveguide-based orthomode transducers. Beam-switching at 1 kHz on the sky is achieved with a fast Faraday rotation polarization switch and a wire-grid to interchange the reflected and transmitted beams to each receiver (see Figure 10). This ultra-wideband receiver typically achieves noise temperatures < 50K between 73 – 111 GHz. Because of the fast beam-switch involving no moving mechanical parts, the Redshift Search Receiver has exceptional baseline stability, well-suited to the detection of redshifted transitions of the CO ladder from star-forming galaxies at cosmological distances. An innovative wideband analog autocorrelator system which covers the full 38 GHz with 31 MHz (100 km s^{-1} at 90 GHz) resolution serves as the backend spectrometer. The 38 GHz of total bandwidth is analyzed in six different slightly overlapping frequency bands (see Figure 12). Table 1 summarizes the capabilities of the RSR system.

The RSR was first commissioned on the FCRAO 14-m telescope in 2006, and in June 2011 it was used to conduct the first-light scientific demonstration observations of the LMT. A python based data reduction program, `DREAMPY` is available to combine and average RSR observations across the multiple frequency bands and multiple pixels into calibrated output spectra. The RSR also features continuum observation capabilities, which are primarily used for pointing and focusing.

Item	Specification	Comment
RF Frequency Range	73 – 111 GHz	Entire 38 GHz band detected simultaneously
Number of Beams	2	Typically Source in one beam and Reference in other
Number of Polarizations	2	Linear
T_R (Receiver Noise)	50 K	Typical
Beam Switch Frequency	1 kHz	Electronic beam switch
Number of Spectra	4	Each observation produces 4 independent 38 GHz wide spectra that can be averaged together

Table 1. RSR Specifications

5.2 SEQUOIA

SEQUOIA is a cryogenic focal plane array of 16 pixels,[18] arranged in a 4×4 array that operates in the RF frequency range of 85 – 115 GHz. The array, which is fed by square horns separated by $2f\lambda$, is cooled to 18 K, and

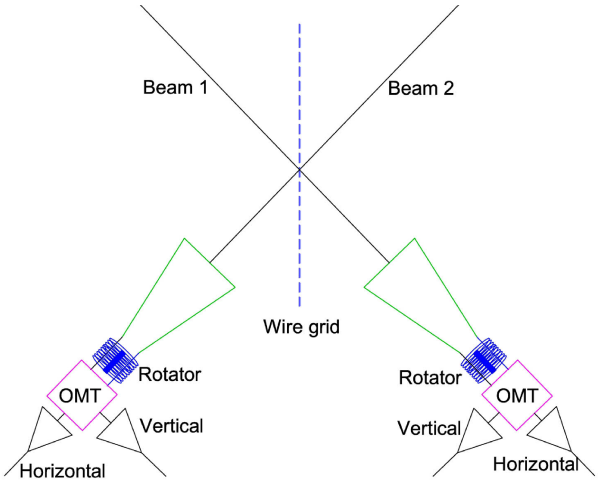

Figure 10. Block diagram of the RSR showing two beams on the sky. The orthogonal polarizations from both spots on the sky (see also Figure 11) make its way to four separate receiver outputs, and four independent spectral backends that produce four independent switched spectra that can be averaged together.

Figure 11. RSR beams are separated on the sky by $\sim 78''$ (~ 5 times HPBW). At any given instant, as the 1 kHz beam switch changes sign, the two orthogonal polarizations in each beam are received by four independent pixels.

uses low-noise Indium Phosphide (InP) monolithic microwave integrated circuit (MMIC) preamplifiers designed at UMass. The characteristic receiver noise temperature is 55 K in the range of 85–107 GHz, and increases to 90 K at 115 GHz. The intermediate frequency (IF) is 5 – 20 GHz for a total of 15 GHz (see Figure 13). Table 2 summarizes the specifications for SEQUOIA.

SEQUOIA was the workhorse facility instrument for the FCRAO 14-m telescope for many years. Installed at the LMT in 2017, the refurbished SEQUOIA has a new digital spectrometer with total bandwidth options of 200, 400, and 800 MHz. All pixels of the array track the same frequency window, so nominally a single spectral line is observed at a time by the array. However, we note that in some cases two lines may fall within the same spectral window so that they may be imaged simultaneously (e.g. HCO^+ J=1-0 and HCN J=1-0 in the 800 MHz bandwidth mode of the spectrometer). A future upgrade of the spectrometer in 2021 will allow the detection of two lines simultaneously in a 15 GHz IF band.

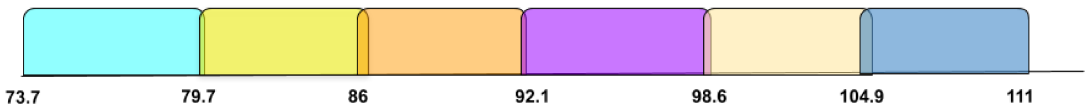

Figure 12. The six different frequency bands of the RSR. Each band which is ~ 6.7 GHz wide is handled by a separate analog auto-correlation card. Four separate chassis handle the entire 38 GHz from each of the four RSR pixels.

Item	Specification	Comment
RF Frequency Range	85 – 115.5 GHz	Available in two frequency bands,
85 –		100 GHz or 100 – 115 GHz
IF Frequency Range	5 – 20 GHz	Up to 800 MHz band within this frequency range available for spectrometers
T_R (receiver noise temperature)	55–90 K	Most of the band is below 60K
Number of beams	4×4 (16 single polarization)	Array footprint rotates on sky as elevation angle changes
Spectrometer Modes	800 MHz (2048 channels), 400 MHz (4096 channels), 200 MHz (8192) channels)	Spectrometer can be placed at any frequency within a 15 GHz IF band

Table 2. SEQUOIA Receiver Specifications

A data reduction pipeline (`LMTSLR` - LMT Spectral Line Reduction) is available for the reduction of spectral line data from SEQUOIA, including regridding of On-the-Fly (OTF) map mode data obtained with SEQUOIA on the LMT. Output data products are in the form of FITS data cubes.

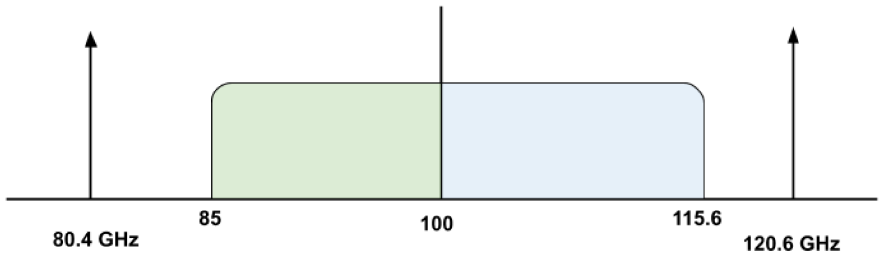

Figure 13. SEQUOIA has two LO frequency options. Depending on whether the 80.4 or 120.6 GHz LO is chosen the band of 85.4–100.4 GHz or 100.6–115.6GHz is sent down to the 5–20 GHz IF band.

5.3 1.3mm EHT Receiver

The single-pixel 1.3mm band receiver is a dual-polarization sideband-separation receiver that operates in the frequency range of 210 – 280 GHz. The receiver is primarily used for VLBI observations with the Event Horizon Telescope (EHT) array, but is also available for general astronomical use at the LMT. The receiver uses superconducting junctions, and features ALMA Band-6 mixer-preamplifiers. Table 3 lists the specifications of the receiver. The cryostat is cooled to 4 Kelvin, and has a square corrugated feed horn followed by an orthomode transducer (OMT) which splits the two polarizations into two separate mixer-preamplifiers. Each of these polarizations further separate the upper and lower sidebands of the intermediate frequency (IF) of 4 – 12 GHz (see Figure 14). In all four separate IF bands are available simultaneously and are fed into a spectrometer system. The orthogonal polarizations can be averaged together for each sideband. The receiver was designed and built at UMass, and provides characteristic receiver noise temperature of 60-75 K across the 210 – 280 GHz band. A flexible computer controlled local oscillator (LO) system allows tuning across the RF frequency range.

The 1.3mm receiver is coupled with the SEQUOIA IF processor and the SEQUOIA spectrometer system. When not used for EHT observations, this receiver can be used with SEQUOIA spectrometer to observe two different molecular transitions in each separated sideband with one of three possible spectrometer modes (see Figure 14 and Table 3).

5.4 OMAyA

The 1mm wavelength window has excellent transmission on the LMT (see Figure 15), and will be the work-horse band for molecular line spectroscopic observations of significant molecular line species in the interstellar medium.

Item	Specification	Comment
RF Frequency	210–280 GHz	ALMA Band-6 Spec
Number of Polarizations	2	
Sidebands	Two Separated Sidebands	
Image Rejection Ratio	> 15 dB	
T_R (receiver noise SSB)	60–75 K	ALMA Band-6 Spec
Spectrometer Modes	800 MHz (2048 channels), 400 MHz (4096 channels), 200 MHz (8192) channels)	Spectrometer can be placed at any frequency within a 15 GHz IF band

Table 3. 1.3 mm band Receiver Specifications

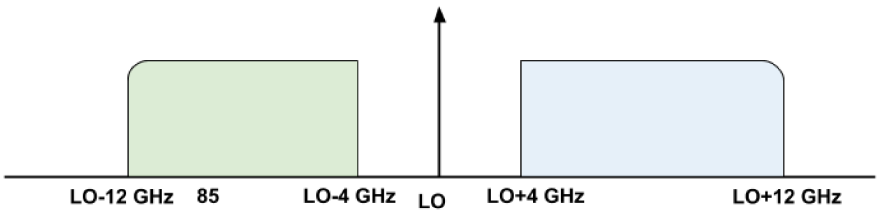

Figure 14. 1.3 mm band Receiver. The local oscillator (LO) can be tuned between 220 to 270 GHz. At each LO setting the upper sideband (USB) and lower sideband (LSB) of the LO setting is separated out and sent to separate IF streams. So molecular lines in each sideband can be separately observed.

OMAyA (One Millimeter Array for Astronomy) is a 8-pixel, dual polarization, sideband separation focal-plane array receiver being built as a facility instrument for the LMT under NSF ATI funding. The array is arranged in a 4×2 configuration on the sky with eight beams at $\sim 14''$ separation. Each pixel of the receiver detects two orthogonal polarizations, and in each polarization, sideband separation super-conducting mixers are employed that separates the two sidebands. In all 32 distinct IF outputs each of which is 8 GHz wide is made available from the receiver. These are coupled to individual spectrometers to produce 32 distinct spectra per observation.

OMAyA is based on heritage from the ALMA Band-6 mixer development.[19] In collaboration with NRAO and the University of Virginia, UMass has fabricated wafers of SIS (superconductor insulator superconductor) junctions. From these junctions, matched sets (with similar current-voltage characteristics) have been identified for use in the OMAyA mixers. OMAyA features eight integrated dual-polarization, sideaband separation mixer blocks (see Figure 16), where the horn section has been integrated with a orthomode transducer (OMT) that splits the input signal into two orthogonal linear polarizations. Each polarization is then fed into a 2SB (sideband separation) mixer arrangement with waveguide hybrids, LO coupler, and super-conducting IF hybrids. This novel design for the integrated system allows the mixer block to be compact, yet produce four distinct IFs in each beam of OMAyA. After further downstream processing, the OMAyA IFs are sent to the same spectrometer system as used in SEQUOIA capable of three different bandwidth modes (800 MHz, 400 MHz, or 200 MHz total bandwidths). OMAyA features an integrated solid-state phase-locked local oscillator (LO) system that allows for computer-controlled tuning of the receiver over the entire RF frequency range. Table 4 summarizes the specifications of the OMAyA receiver. As with SEQUOIA, the `LMTSLR` data reduction package will be used with OMAyA and OTF mapping observations to produce final regridded spectral line data cubes.

The OMAyA integrated mixer blocks and the horn array have been fabricated and are being assembled in the UMass receiver lab. The Covid-19 pandemic has slowed the assembly and testing of the instrument due to reduced access for laboratory activities over significant times in 2020. However, we expect to complete assembly, testing, installation and commissioning of OMAyA by Fall 2021.

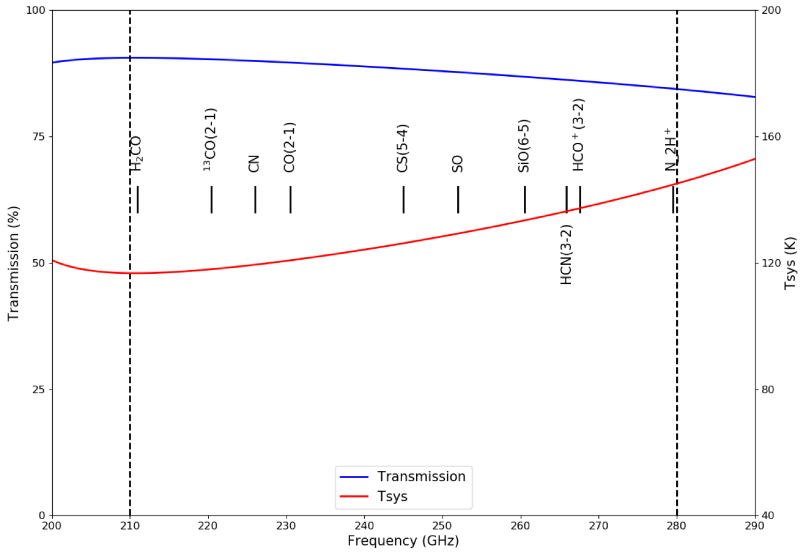

Figure 15. Atmospheric tranmission and system temperature for OMAyA in the 1mm wavelength atmospheric window. Shown also are a few astrophysically significant molecular species that is accessible with the OMAyA instrument.

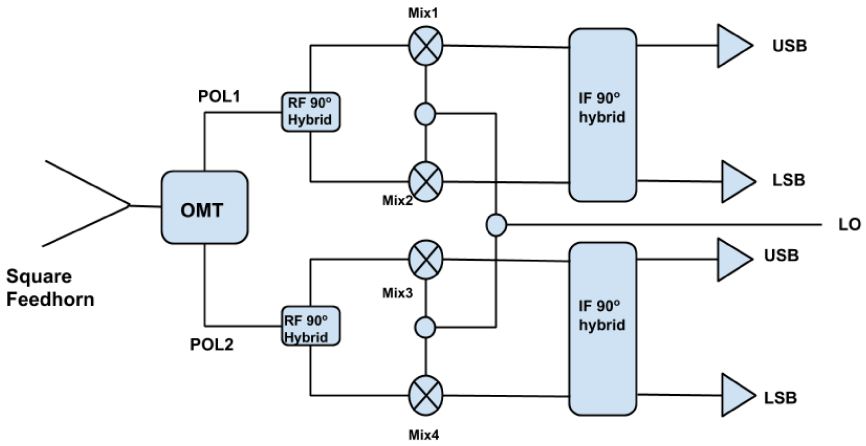

Figure 16. Block Diagram of an individual OMAyA mixer block. The OMAyA focal plane consists of 8 of these integrated mixer blocks. A square corrugated feed-horn feeds an orthomode transducer (OMT) which splits the orthogonal linear polarizations into two output waveguide. In each polarization, a RF 90° hybrid, a LO 0° 3 dB splitter, two SIS junction based mixers, and an IF 90° hybrid together forms a 2SB (sideband separation) mixer arrangement that splits the upper and lower sidebands into two separate bands, which are then amplified by cryogenic low-noise IF amplifiers and sent to the IF processor for further processing.

5.5 The TolTEC Camera

The TolTEC camera is a 3-band imaging polarimeter being built as a facility instrument for the LMT under funding from the NSF/MSIP program. The camera utilizes 7718 kinetic inductance detectors (KIDs) in three arrays to provide simultaneous imaging in bands centered at 1.1 mm, 1.4 mm, and 2.0 mm wavelength. The active pixel count of the camera, when combined with the 50 m diameter LMT, will result in a combination of mapping speed and resolution that is unmatched by any other millimeter-wavelength facility. An overview of the

Item	Specification	Comment
Number of Beams	4×2	Beam Separation $\sim 14''$
Number of Polarizations	2	in each beam
Number of Sidebands	2	32 total output IFs
RF Frequency Range	210–280 GHz	
IF Frequency Range	4–12 GHz	
T_{rmR} (receiver noise temperature)	60–75 K	
Spectrometer Modes	800 MHz - 2048 channels	Resolution 0.5 km s^{-1} at 230 GHz
	400 MHz - 4096 channels	Resolution 0.12 km s^{-1} at 230 GHz
	200 MHz - 8192 channels	Resolution 30 ms^{-1} at 230 GHz

Table 4. OMAyA Specifications

TolTEC camera design and in-lab performance is given in paper in these proceedings.[20] Additional contributions include a paper on TolTEC's software architecture,[21] detectors[22] and optical design.[23]

The optical design and sensitivity estimates for TolTEC were originally described in Bryan *et al.* 2018.[24] Table 5 provides the key features and sensitivity calculations for the camera.

Once installed on the LMT, the TolTEC Project will undertake a series of ten Legacy Surveys, each using 100 hours of telescope time, whose data will be made publicly available. The first four of these surveys were designed through a series of public webinars and meetings in 2018.[25] They are: the Fields in Filament Survey - a survey of the magnetic fields via polarized dust emission in star-forming regions; the Clouds to Cores Survey - a survey of the core mass function in several molecular clouds; the Ultra-Deep Survey - a survey of metal production and star formation in galaxies at the 1.1mm confusion limit; and the Large Scale Structure Survey - a survey of the distribution and prevalence of ULIRGs and SMGs over 50 deg^2.

The full TolTEC instrument was integrated and has been undergoing testing at UMass since late 2019. A subtle but vexing problem with the dichroic beam splitters, which we ultimately traced to a fabrication issue, required a series of cooldowns and optical tests of the instrument during much of 2020. In addition, the Covid-19 pandemic led to a shutdown of instrument hardware activities for 3 months of 2020 followed by a reduced level of person-power in the lab for testing. Consequently, we now expect to ship TolTEC to the LMT in 2021, once the Covid-19 pandemic allows, for commissioning and first science.

Parameter	2.1mm	1.4mm	1.1mm	Notes
Beam Size	9.5	6.3	5.0	FWHM in arcseconds
NEFD	0.59	1.0	1.46	detector point source sensitivity in mJy$\sqrt{s}$
NEP	50	72	95	noise equivalent power (at detector)
# Detectors	1172	2532	4012	
Mapping Speed	**13.7**	**4.4**	**2.1**	$Deg^2/mJy^2/hr$

Table 5. TolTEC/LMT parameters. The point-source mapping speeds are calculated as in[24] using a combination of detector predictions and *measured* performance of the LMT, scaled from 32m to the 50m telescope configuration. For all calculations we assume a 225GHz opacity of 0.1 (the median at the LMT site in the winter) and a zenith angle of 30 degrees.

ACKNOWLEDGMENTS

We gratefully acknowledge the Consejo Nacional de Ciencia y Tecnología (CONACYT) for their support of the operation and maintenance of the LMT with grants - U0004-246083, U0004-259839, F0003-272050, M0037-279006 and F0003-281692, and the National Science Foundation grants for their recent support of LMT performance development (AST-1935980), as well as development of the following facility instruments: RSR (AST-0096854 and AST-0704966, AST-0704966), OMAYA (AST-1507267), Rx1.3mm (AST-1440254) and TolTEC (AST-1636621).

REFERENCES

[1] Zeballos, M., Ferrusca, D., Contreras R., J., and Hughes, D. H., "Reporting the first 3 years of 225-GHz opacity measurements at the site of the Large Millimeter Telescope Alfonso Serrano," in [*Ground-based and Airborne Telescopes VI*], Hall, H. J., Gilmozzi, R., and Marshall, H. K., eds., *Society of Photo-Optical Instrumentation Engineers (SPIE) Conference Series* **9906**, 99064U (July 2016).

[2] Schloerb, F., Souccar, K., Chávez Dagostino, M., Ferrusca Rodriguez, D., Gale, D., Gómez-Ruiz, A., Hughes, D., Wilson, G., and Sanchez-Arguelles, D., "Moving towards daytime observing at the Large Millimeter Telescope," in [*Ground-based and Airborne Telescopes VIII*], Marshall, H., Spyromilio, J., and Usuda, T., eds., *Society of Photo-Optical Instrumentation Engineers (SPIE) Conference Series* **11445**, 11445–217 (2020).

[3] Gale, D. M., Schloerb, F. P., León Huerta, A., Lucero Álvarez, M., Cabrera Cuevas, L., Tecuapetla Sosa, E., Castro Santos, D., Tzile Torres, C., and Hernández Rios, E., "Photogrammetry mapping and alignment of the LMT 50-meter primary reflector," in [*Advances in Optical and Mechanical Technologies for Telescopes and Instrumentation III*], Navarro, R. and Geyl, R., eds., *Society of Photo-Optical Instrumentation Engineers (SPIE) Conference Series* **10706**, 1070646 (July 2018).

[4] Valsecchi, G., Banham, R., Bianucci, G., Eder, J., Ghislanzoni, R., Ritucci, A., Terraneo, M., Zocchi, F. E., Smith, D., Gale, D., and Hughes, D., "A segmented subreflector with electroformed nickel laminated panels for the Large Millimeter Telescope," in [*Advances in Optical and Mechanical Technologies for Telescopes and Instrumentation II*], Navarro, R. and Burge, J. H., eds., *Society of Photo-Optical Instrumentation Engineers (SPIE) Conference Series* **9912**, 99123P (July 2016).

[5] Smith, D. R., Souccar, K., Gale, D. M., Lucero Álvarez, M., Hernández Rios, E., Olmos Tapia, A., Moreno Nolasco, M. E., Cuq, M., Noire, P., Pawlowski, R., and Roux, T., "Factory characterization testing of a large precision hexapod for the LMT/GTM," in [*Advances in Optical and Mechanical Technologies for Telescopes and Instrumentation III*], Navarro, R. and Geyl, R., eds., *Society of Photo-Optical Instrumentation Engineers (SPIE) Conference Series* **10706**, 1070649 (July 2018).

[6] Souccar, K., Wallace, G., and Malin, D., "A reusable automatically generated software system for the control of the Large Millimeter Telescope," in [*Advanced Telescope and Instrumentation Control Software II*], Lewis, H., ed., *Society of Photo-Optical Instrumentation Engineers (SPIE) Conference Series* **4848**, 35–42 (Dec. 2002).

[7] Souccar, K., Wallace, G., and Malin, D., "A standard control system for the Large Millimeter Telescope and instruments," in [*Advanced Software, Control, and Communication Systems for Astronomy*], Lewis, H. and Raffi, G., eds., *Society of Photo-Optical Instrumentation Engineers (SPIE) Conference Series* **5496**, 241–249 (Sept. 2004).

[8] Souccar, K. and Smith, D., "The architecture and initial results of the Large Millimeter Telescope control system," in [*Ground-based and Airborne Telescopes II*], Stepp, L. M. and Gilmozzi, R., eds., *Society of Photo-Optical Instrumentation Engineers (SPIE) Conference Series* **7012**, 701209 (July 2008).

[9] Smith, D. R. and Souccar, K., "Main axis control of the Large Millimeter Telescope," in [*Ground-based and Airborne Telescopes III*], Stepp, L. M., Gilmozzi, R., and Hall, H. J., eds., *Society of Photo-Optical Instrumentation Engineers (SPIE) Conference Series* **7733**, 77332M (July 2010).

[10] Arteaga Magaña, C., Smith, D. R., and Hernández Rebollar, J. L., "Mechanical improvement of the interim LMT/GTM primary surface actuators," in [*Advances in Optical and Mechanical Technologies for Telescopes and Instrumentation*], Navarro, R., Cunningham, C. R., and Barto, A. A., eds., **9151**, 802 – 811, International Society for Optics and Photonics, SPIE (2014).

[11] Smith, D. R., Souccar, K., Arteaga Magaña, C., Montalvo, G., and Hernández Rebollar, J. L., "Performance testing of the LMT/GTM primary surface actuators," in [*Advances in Optical and Mechanical Technologies for Telescopes and Instrumentation*], Navarro, R., Cunningham, C. R., and Barto, A. A., eds., *Society of Photo-Optical Instrumentation Engineers (SPIE) Conference Series* **9151**, 91512C (July 2014).

[12] Schloerb, F. P., Sanchez, D., Narayanan, G., Erickson, N., Souccar, K., Wilson, G., Gale, D., Hughes, D. H., and Smith, D., "Calibration and operation of the active surface of the Large Millimeter Telescope," in [*Ground-based and Airborne Telescopes VI*], Hall, H. J., Gilmozzi, R., and Marshall, H. K., eds., *Society of Photo-Optical Instrumentation Engineers (SPIE) Conference Series* **9906**, 99066C (Aug. 2016).

[13] Smith, D. R., Souccar, K., Montalvo, G., Arteaga Magaña, C., Hernández Rebollar, J. L., Olmos Tapia, A., Gallieni, D., Lazzarini, P., Fumi, P., and Anaclerio, E., "Laboratory and field testing results of the LMT/GTM primary surface actuators," in [*Advances in Optical and Mechanical Technologies for Telescopes and Instrumentation II*], Navarro, R. and Burge, J. H., eds., *Society of Photo-Optical Instrumentation Engineers (SPIE) Conference Series* **9912**, 991214 (July 2016).

[14] Smith, D. R., Souccar, K., Montalvo, G., Arteaga Magaña, C., Hernández Rebollar, J. L., Lázaro Hernández, J., Moreno Nolasco, M. E., Fumi, P., Anaclerio, E., and Gallieni, D., "Field testing and performance characterization of the production LMT/GTM active surface actuators," in [*Advances in Optical and Mechanical Technologies for Telescopes and Instrumentation III*], Navarro, R. and Geyl, R., eds., *Society of Photo-Optical Instrumentation Engineers (SPIE) Conference Series* **10706**, 107066Q (July 2018).

[15] Ruze, J., "Antenna Tolerance Theory – A Review," *IEEE Proceedings* **54**, 633–642 (Apr. 1966).

[16] Stumpff, P., "Astronomische Pointing Theorid Fuer Radioteleskope," *Klein Heubacher Berichte* **15**, 432–437 (1972).

[17] Erickson, N., Narayanan, G., Goeller, R., and Grosslein, R., "An Ultra-Wideband Receiver and Spectrometer for 74–110 GHz," in [*From Z-Machines to ALMA: (Sub)Millimeter Spectroscopy of Galaxies*], Baker, A. J., Glenn, J., Harris, A. I., Mangum, J. G., and Yun, M. S., eds., *Astronomical Society of the Pacific Conference Series* **375**, 71 (Oct. 2007).

[18] Erickson, N. R., Grosslein, R. M., Erickson, R. B., and Weinreb, S., "A cryogenic focal plane array for 85-115 GHz using MMIC preamplifiers," *IEEE Transactions on Microwave Theory Techniques* **47**, 2212–2219 (Dec. 1999).

[19] Kerr, A. R., Pan, S.-K., Claude, S. M. X., Dindo, P., Lichtenberger, A. W., Effland, J. E., and Lauria, E. F., "Development of the ALMA Band-3 and Band-6 Sideband-Separating SIS Mixers," *IEEE Transactions on Terahertz Science and Technology* **4**, 201–212 (Mar. 2014).

[20] Wilson, G., Ade, P., Aretxaga, I., Austermann, J., Ban, Y., Bardin, J., Beall, J., Berthoud, M., Bryan, S., Bussan, J., Castillo-Domínguez, E., Chavez, M., Contente, R., DeNigris, N., Dober, B., Ferrusca, D., Fissel, L., Gao, J., Golec, J., Golina, R., Gomez, A., Gordon, S., Gutermuth, R., Hilton, G., Hosseini, M., Hubmayr, J., Hughes, D., Kuczarski, S., Lunde, E., Ma, Z., Mani, H., Mauskopf, P., McCrackan, M., McKenney, C., McMahon, J., Novak, G., Pisano, G., Sapienza, L., Pope, A., Rodriguez, I., Sánchez-Argüelles, D., Schloerb, F., Simon, S., Sinclair, A., Souccar, K., Torres Campos, A., Tucker, C., Ullom, J., Van Lanen, J., Vissers, M., Van Camp, E., Velazquez, M., Weeks, E., and Yun, M., "The TolTEC camera: an overview of the instrument and in-lab testing results," in [*Millimeter, Submillimeter, and Far-Infrared Detectors and Instrumentation for Astronomy X*], Zmuidzinas, J. and Gao, J.-R., eds., *Society of Photo-Optical Instrumentation Engineers (SPIE) Conference Series* **11453**, 11453–1 (2020).

[21] Ma, Z., McCrackan, M., Denigris, N., Souccar, K., Wilson, G., Horton, P., Lee, D., Mauskopf, P., Novak, G., Rodríguez-Montoya, I., and Zaragoza-Cardiel, J., "The TolTEC data analysis pipeline and software stack ," in [*Software and Cyberinfrastructure for Astronomy VI*], Guzman, J. and Ibsen, J., eds., *Society of Photo-Optical Instrumentation Engineers (SPIE) Conference Series* **11452**, 11452–110 (2020).

[22] Austermann, J., Ban, Y., Beall, J., Berthoud, M., Contente, R., DeNigris, N., Dober, B., Gao, J., Hilton, G., Hubmayr, J., Kuczarski, S., Lee, D., Lunde, E., Ma, Z., Mauskopf, P., McCrackan, M., McKenney, C., McMahon, J., G., N., Abi-Saad, S., Simon, S., Souccar, K., Ullom, J., Van Camp, E., Van Lanen, J., Vissers, M., and Wilson, G., "TolTEC focal plane arrays: design, characterization, and performance of kilopixel MKID focal planes," in [*Millimeter, Submillimeter, and Far-Infrared Detectors and Instrumentation for Astronomy X*], Zmuidzinas, J. and Gao, J.-R., eds., *Society of Photo-Optical Instrumentation Engineers (SPIE) Conference Series* **11453**, 11453–10 (2020).

[23] Lunde, E., Ade, P., Berthoud, M., Contente, R., DeNigris, N., Doyle, S., Ferrusca, D., Golec, J., Kuczarski, S., Lee, D., Mauskopf, P., McMahon, J., Simon, S., Novak, G., Tucker, C., Underhill, M., Van Camp, E., and Wilson, G., "The optical design and performance of TolTEC: A millimeter-wave imaging polarimeter," in [*Millimeter, Submillimeter, and Far-Infrared Detectors and Instrumentation for Astronomy X*], Zmuidzinas, J. and Gao, J.-R., eds., *Society of Photo-Optical Instrumentation Engineers (SPIE) Conference Series* **11453**, 11453–5 (2020).

[24] Bryan, S., Austermann, J., Ferrusca, D., Mauskopf, P., McMahon, J., Montaña, A., Simon, S., Novak, G., Sánchez-Argüelles, D., and Wilson, G., "Optical design of the TolTEC millimeter-wave camera," in [*Millimeter, Submillimeter, and Far-Infrared Detectors and Instrumentation for Astronomy IX*], Zmuidzinas, J. and Gao, J.-R., eds., *Society of Photo-Optical Instrumentation Engineers (SPIE) Conference Series* **10708**, 107080J (July 2018).

[25] Montaña, A., Chávez Dagostino, M., Aretxaga, I., Novak, G., Pope, A., Wilson, G., and TolTEC Team, "TolTEC: unveiling the hidden universe.," *Memorie della Societa Astronomica Italiana* **90**, 632 (Jan. 2019).